DYNAMICS OF A STRONGLY NONLINEAR SPACECRAFT STRUCTURE PART I: EXPERIMENTAL IDENTIFICATION

J.P. Noël, L. Renson, and G. Kerschen

Space Structures and Systems Lab
Aerospace and Mechanical Engineering Department, University of Liège
1, Chemin des chevreuils (B52/3), 4000, Liège, Belgium
jp.noel, l.renson, g.kerschen@ulg.ac.be

ABSTRACT

The present paper addresses the identification of a real-life spacecraft structure possessing a strongly nonlinear component with multiple mechanical stops. The complete identification procedure, from nonlinearity detection and characterization to parameter estimation, is carried out based upon experimental sine-sweep data collected during a classical spacecraft qualification campaign.

Key words: Spacecraft structure; experimental data; nonlinear system identification; modal interactions.

1. INTRODUCTION

Nonlinear system identification is a challenging task in view of the complexity and wide variety of nonlinear phenomena. Significant progress has been enjoyed during the last fifteen years or so [KWVG06] and, to date, multi-degree-of-freedom lumped-parameter systems and simple continuous structures with localized nonlinearities are within reach. The identification of weak nonlinearities in more complex systems was also addressed in the recent past. The identification of large-scale structures with multiple, and possibly strongly, nonlinear components nevertheless remains a distinct challenge and concentrates current research efforts.

The present paper addresses the identification of the SmallSat spacecraft developed by EADS-Astrium, which possesses a vibration isolation device with multiple mechanical stops. The complete identification procedure, from nonlinearity detection and characterization to parameter estimation [KWVG06], will be achieved based upon experimental sine-sweep data collected during a classical spacecraft qualification campaign. Throughout the paper, the combined use of analysis techniques will bring different perspectives to the dynamics. Specifically, the spacecraft will be shown to exhibit particularly interesting nonlinear behaviors, including jumps and modal interactions. Specific attention will be devoted to nonlinear modal interactions as their experimental evidence in the case of a complex, real-life structure is an important contribution of this work. Note that a thorough numerical study of the SmallSat satellite dynamics is carried out in a companion paper [RNK14].

2. THE SMALLSAT SPACECRAFT STRUCTURE

The SmallSat structure was conceived by EADS-Astrium as a low-cost platform for small satellites in low earth orbits. It is a monocoque tube structure which is 1.2 m in height and 1 m in width. It is composed of eight flat faces for equipment mounting purposes, creating an octagon shape, as shown in Fig. 1. The top floor is an 1-m^2 sandwich aluminum panel. The interface between the spacecraft and the launch vehicle is achieved via four aluminum brackets located around cut-outs at the base of the structure. The total mass including the interface brackets is around 64 kg.

The spacecraft structure supports a dummy telescope mounted on a baseplate through a tripod; its mass is around 140 kg. The dummy telescope plate is connected to the SmallSat top floor by three shock attenuators, termed shock attenuation systems for spacecraft and adaptor (SASSAs). Besides, as depicted in Fig. 2 (a), a support bracket connects to one of the eight walls the so-called wheel elastomer mounting system (WEMS) device which is loaded with an 8-kg dummy inertia wheel. The WEMS device acts as a mechanical filter which mitigates high-frequency disturbances coming from the inertia wheel through the presence of a soft elastomeric interface between its mobile part, *i.e.* the inertia wheel and a supporting metallic cross, and its fixed part, *i.e.* the bracket and by extension the spacecraft. Moreover, the WEMS incorporates eight mechanical stops, covered with a thin layer of elastomer, and designed to limit the axial and lateral motions of the inertia wheel during launch, which gives rise to strongly nonlinear dynamical phenomena.

Fig. 2 (b) presents a simplified, yet relevant, modeling

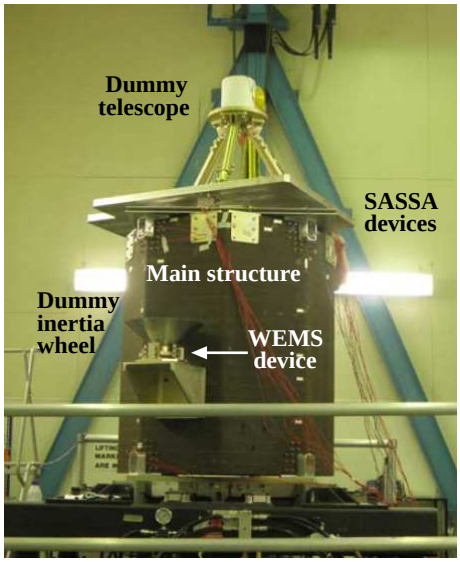

Figure 1: SmallSat spacecraft equipped with an inertia wheel supported by the WEMS device and a dummy telescope connected to the main structure by the SASSA isolators.

of the WEMS device where the inertia wheel, owing to its important rigidity, is seen as a point mass. The four nonlinear connections (NCs) between the WEMS mobile and fixed parts are labeled NC 1 – 4. Each NC possesses a trilinear spring in the axial direction (elastomer in traction/compression plus two stops), a bilinear spring in the radial direction (elastomer in shear plus one stop), and a linear spring in the third direction (elastomer in shear). The stiffness and damping properties of the WEMS were estimated during experiments carried out by EADS-Astrium at subsystem level (see Table 1), and will serve as reference values in this study. For confidentiality, stiffness coefficients and clearances are given through adimensionalised quantities.

	Lateral X and Y	Axial Z
Stiff. coeff. of the elast. plots	2	8
Stiff. coeff. of the mech. stops	40	100
Clearance	2	1.5
Damp. coeff. of the elast. plots (Ns/m)	37	63

Table 1: Reference stiffness and damping properties of the WEMS device estimated during experiments carried out by EADS-Astrium at subsystem level.

Low-level random data were acquired throughout the test campaign, specifically between each qualification run, to monitor the integrity of the structure. This was performed considering axial white-noise excitations filtered in 5 – 100 Hz and driven via a base acceleration of 0.001 g^2/Hz. The low-level time series can be exploited to identify the linear modal properties of the spacecraft, utilizing transmissibility functions (TFs) as no force measurement was available at the shaker-to-structure interface. The identification was carried out using a frequency-domain subspace identification algorithm. The resulting estimates of the resonance frequencies and damping ratios of the spacecraft are given in Table 2.

The actual qualification test campaign consisted of swept-sine base excitations applied to the spacecraft for different amplitude levels, sweep rates and directions. Two specific data sets measured under 0.6 g and 1 g axial loadings and for positive sweep rates of 2 and 4 octaves per minute, respectively, are exploited in the present work for nonlinear system identification. For conciseness, their analysis is focused in the next sections on the frequency range between 5 and 15 Hz, *i.e.* the vicinity of the first mode of vibration of the structure. The associated spacecraft motion is depicted in Fig. 3 through the modal coordinates of the inertia wheel and telescope in the X, Y and Z directions. This motion consists mainly in a swing oscillation of the inertia wheel around Y-axis.

Mode	Frequency (Hz)	Damping ratio ($\%$)
1	8.19	4.36
2	20.18	5.21
3	22.45	6.76
4	34.30	5.03
5	43.16	2.76
6	45.99	3.72
7	55.71	3.66
8	64.60	4.78
9	88.24	2.89

Table 2: Linear resonance frequencies and damping ratios estimated using a frequency-domain subspace identification algorithm applied to low-level random data (0.001 g^2/Hz).

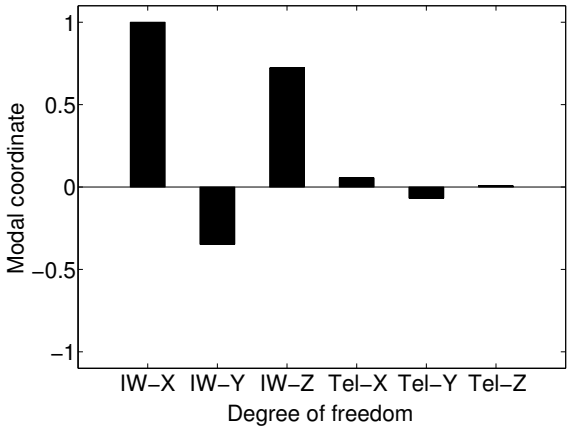

Figure 3: First mode of vibration of the spacecraft described through the modal coordinates of the dummy inertia wheel and telescope in the X, Y and Z directions.

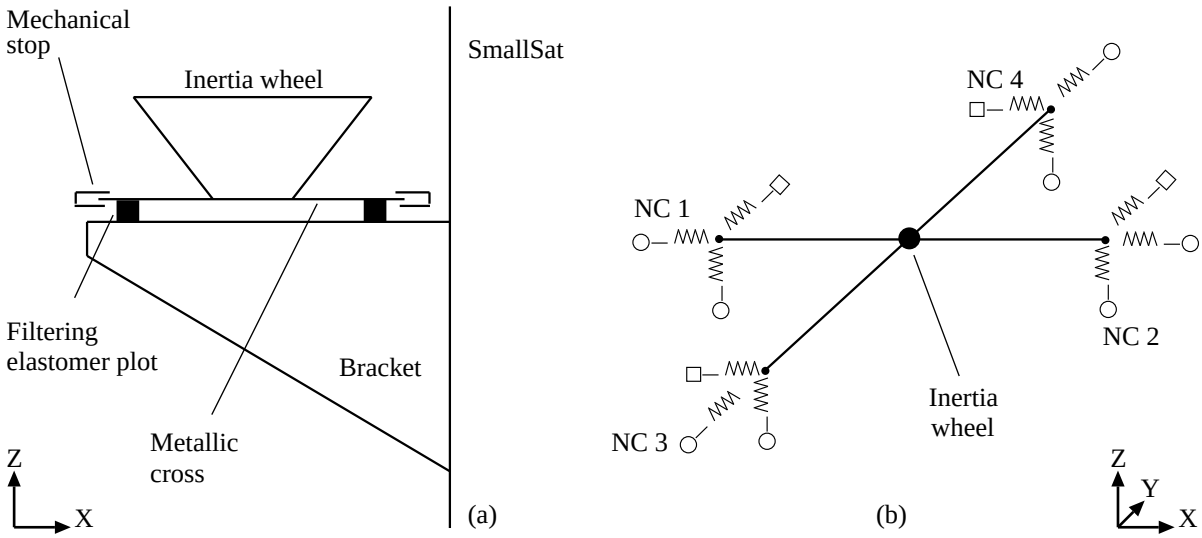

Figure 2: WEMS device. (a) Detailed description of the WEMS components; (b) simplified modeling of the WEMS mobile part considering the inertia wheel as a point mass. The linear and nonlinear connections between the WEMS mobile and fixed parts are signaled by squares and circles, respectively.

3. DETECTION OF NONLINEARITY

Nonlinearity detection is the first step of the identification process [KWVG06], and basically boils down to seeking departures from linear theory predictions. In this regard, stepped- and swept-sine excitations are particularly convenient because, if linear, the structure is known to generate a pure sine wave in output, and distortions may be detected without requiring complicated post-processing.

3.1. Envelope-based analysis of the raw time series

Nonlinear distortions in response to sine excitations can sometimes be such that a mere visual inspection of the raw time series is sufficient to reveal nonlinear behavior. To this end, the axial relative displacements across NC 1 measured at 0.6 g and 1 g are plotted in Fig. 4 (a – b), respectively. Note that the measured accelerations were integrated twice using the trapezium rule and then high-pass filtered to obtain displacement signals. For confidentiality, relative displacements and velocities are adimensionalised throughout the paper.

The first observation is the absence of proportionality between the time responses in Fig. 4 (a – b). This is especially visible for negative displacements where the maximum amplitude reached at 0.6 g and 1 g is almost unchanged. This violates the principle of superposition, a cornerstone of the linear theory. The location of the resonance in amplitude in the two graphs can also be seen to be shifted towards higher frequencies, from 8.3 to 9 Hz as the level is increased from 0.6 to 1 g. One further remarks the clear skewness and nonsmoothness of the envelope of oscillations in Fig. 4 (b), which exhibits a sudden transition from large to small amplitudes of vibration, referred to as a jump phenomenon. This envelope also presents a significant asymmetry entailing larger amplitudes of motion in positive displacement, and a discontinuity in slope for negative displacements around 7.5 Hz.

By contrast, the envelope of response at 0.6 g shows no evidence of nonlinear distortion. However, analyzing the response in the vicinity of resonance, *i.e.* in the 8.1 – 8.4 Hz interval, as presented in Fig. 4 (c), highlights the presence of harmonics in the time series. A similar inspection at 1 g, depicted in Fig. 4 (d) in 8.4 – 8.7 Hz, reveals much more significant harmonics and a limitation of the amplitude of motion in negative displacement resulting in the aforementioned asymmetry of the response.

4. CHARACTERIZATION OF NONLINEARITY

Nonlinearity characterization is the second step of the identification process, and amounts to selecting appropriate functional forms to represent the nonlinearities in the system. Characterization is of paramount importance, as the success of the third step of the process, *i.e.* the estimation of model parameters, is conditional upon a precise understanding of the nonlinear mechanisms involved. It is also a very challenging step because the physical phenomena that entail nonlinearity are numerous and may result in plethora of dynamic behaviors.

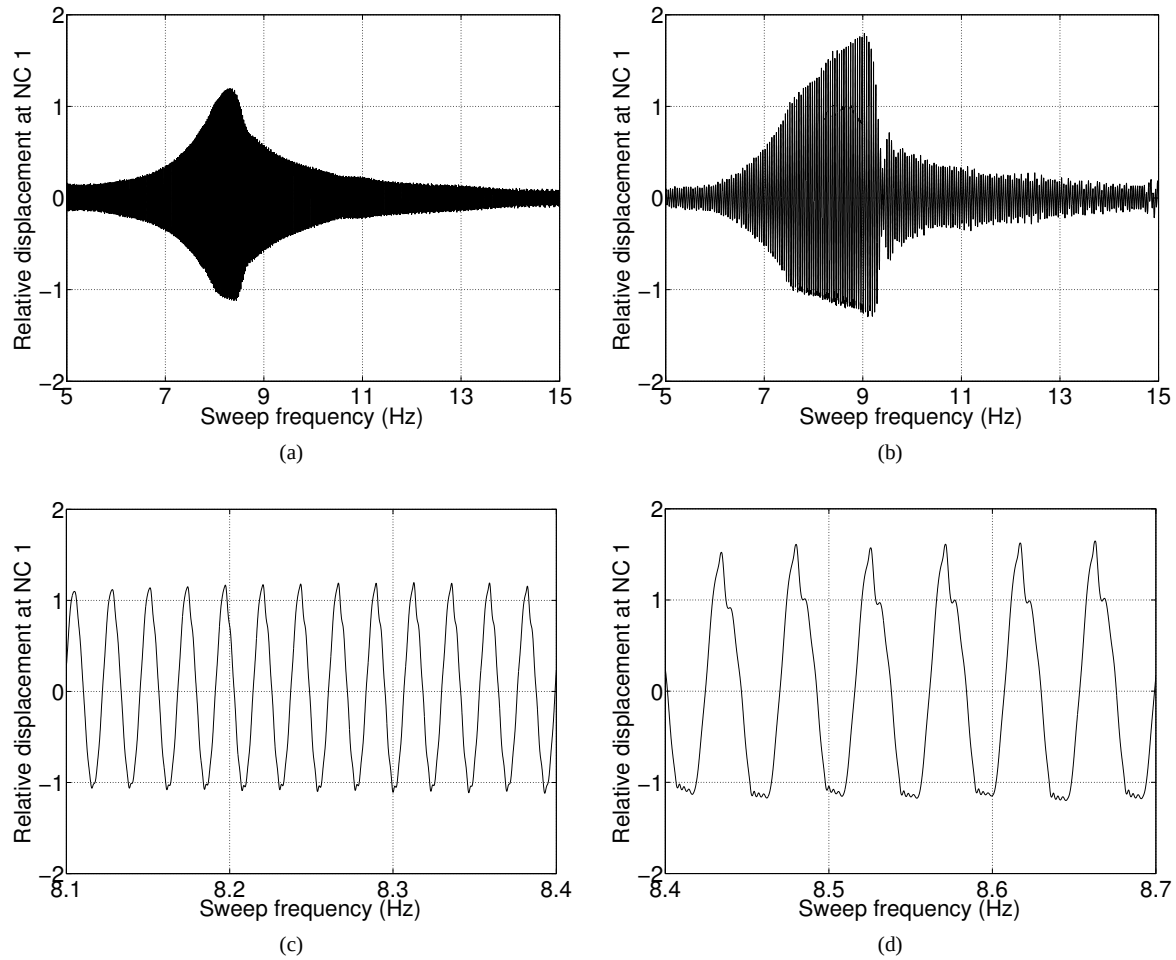

Figure 4: Nonlinearity detection at 0.6 g (left column) and 1 g (right column). (a – b) Envelope-based analysis; (c – d) close-up of the displacement signals.

4.1. Restoring force surface plots

The restoring force surface (RFS) method [KWVG06] serves commonly as a parameter estimation technique, as in Section 5 of the present paper. This section introduces an unconventional use of the RFS method for nonlinearity characterization purposes, relying exclusively on measured signals. The starting point is Newton's second law of dynamics written for a specific degree of freedom (DOF) located next to a nonlinear structural component, namely

$$\sum_{n=1}^{N} m_{i,n}\,\ddot{q}_n + f_i(\mathbf{q},\dot{\mathbf{q}}) = p_i \qquad (1)$$

where i is the DOF of interest, N the number of DOFs in the system, $m_{i,j}$ the mass matrix elements, $\mathbf{q}$, $\dot{\mathbf{q}}$ and $\ddot{\mathbf{q}}$ the displacement, velocity and acceleration vectors, respectively, $\mathbf{f}$ the restoring force vector encompassing elastic and dissipative effects, and $\mathbf{p}$ the external force vector. The key idea of the approach is to discard in Eq. (1) all the inertia and restoring force contributions that are not related to the nonlinear component, as they are generally either unknown, *e.g.* the coupling inertia coefficients, or not measured, *e.g.* the rotational DOFs. If we denote by j another measured DOF located across the nonlinear connection, Eq. (1) is therefore approximated by

$$m_{i,i}\,\ddot{q}_i + f_i(q_i - q_j, \dot{q}_i - \dot{q}_j) \approx p_i. \qquad (2)$$

If no force is applied to DOF i, a simple rearrangement leads to

$$f_i(q_i - q_j, \dot{q}_i - \dot{q}_j) \approx -m_{i,i}\,\ddot{q}_i. \qquad (3)$$

Eq. (3) shows that the restoring force of the nonlinear connection is approximately proportional to the acceleration at DOF i. Hence, by simply representing the acceleration signal, with a negative sign, measured at one side of the nonlinear connection as a function of the relative displacement and velocity across this connection, the nonlinearities can be conveniently visualized, and an adequate mathematical model for their description can then be selected.

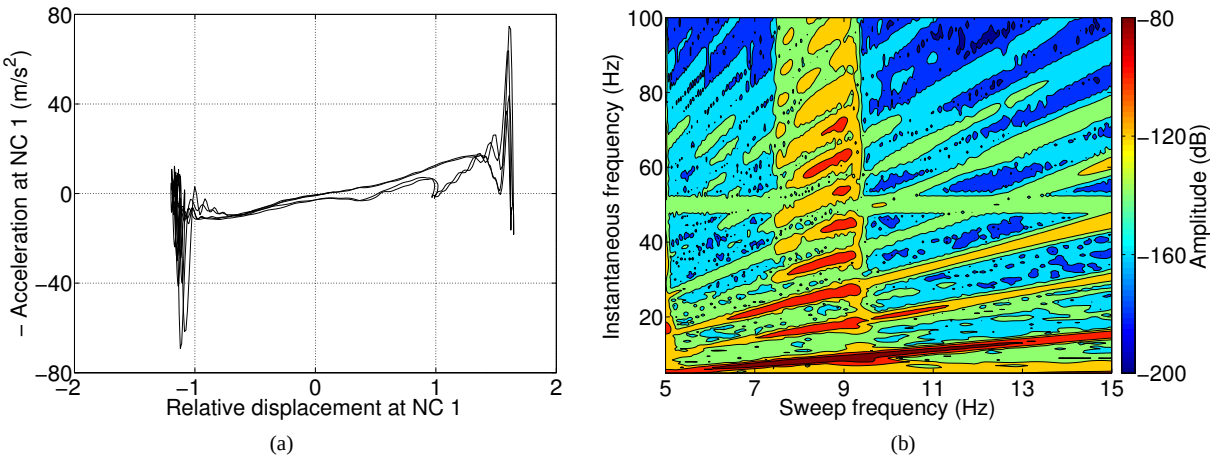

Figure 5: Nonlinearity characterization of the WEMS device at 1 g using (a) the restoring force surface method and (b) the wavelet transform.

To visualize the elastic nonlinearities of the WEMS device, a cross section along the axis where the velocity is zero of the restoring force surface defined by the triplets $(q_{i,k} - q_{j,k},\, \dot{q}_{i,k} - \dot{q}_{j,k},\, -\ddot{q}_{i,k})$, where k refers to the k-th sampled instant, can be drawn. Fig. 5 (a) shows the plot corresponding to NC 1 at 1 g. This figure is particularly useful as it reaffirms the nonsmooth and asymmetric nature of the nonlinearities in the system, and the estimation of the – Z clearance at around 1. It also reveals the activation of the + Z stop, beyond a relative displacement of about 1.5.

4.2. Time-frequency analysis using the wavelet transform

One of the most suitable tools for interpreting harmonics generated by nonlinear systems in response to swept-sine excitations is the wavelet transform (WT) [Sta00]. The wavelet amplitude of the relative displacement of Fig. 4 (b) is displayed in logarithmic scaling in Fig. 5 (b). The appearance of wideband frequency components around 7.5 Hz, including even harmonics, confirms the activation of a nonsmooth nonlinearity in the neighborhood of the resonance and the existence of an asymmetry in the system. The disappearance of the wideband content is seen to coincide closely with the jump phenomenon observed in Fig. 4 (b). One should also point out that impurities in the input sine wave turn into weak harmonics visible throughout the spectrum, but hence not attributable to nonlinearity. Similarly, electrical noise is responsible for a polluting frequency line around 50 Hz.

In summary, the nonlinearity characterization step reveals that an accurate representation of the WEMS nonlinear behavior should account for combined nonsmooth and asymmetric effects. This leads us to select a trilinear model with dissimilar clearances for the nonlinearity. No characterization of damping was attempted in this section as the scope of the paper is focused on the identification of the nonlinear dynamics introduced by the WEMS mechanical stops. One therefore opts for a simple linear damping model for the elastomer components of the WEMS.

4.3. Evidence of nonlinear modal interactions

The WT can evidence a salient feature of nonlinear systems that has no counterpart in linear theory, namely modal interactions between well-separated modes [KPGV09]. To reveal nonlinear modal interactions in the SmallSat dynamics, Fig. 6 (a) depicts the wavelet amplitude of the acceleration measured at NC 4 in the Z direction over 5 – 35 Hz. Compared to the wavelet represented in Fig. 5 (b), a linear scale is used herein to focus on the most significant frequency components in the time series. The excitation frequency is clearly seen throughout the wavelet, but higher harmonic components of at least comparable amplitude are also visible. In particular, a significant level of response, encircled in Fig. 6 (a), is observed around 60 Hz for sweep frequencies just below 30 Hz. This corresponds to a 2:1 interaction between two internally resonant modes of the structure, namely mode 3, which involves an out-of-phase motion of the inertia wheel and the WEMS bracket, and mode 7, which consists in an axial motion of the telescope supporting panel. The existence of a 2:1 interaction between modes 3 and 7 is confirmed in Fig. 6 (b) where the raw acceleration signal measured at the center of the instrument panel is plotted at 0.1 g and 1 g. A high amplitude response at 1 g is observed between 20 and 30 Hz, which can be confidently attributed to a nonlinear resonance as no linear mode of the panel is located in this interval. One also remarks the presence of two resonances around 46 and 56 Hz, as predicted by the linear modal analysis carried out in Section 2. At the 0.1 g excitation level for which the satellite behaves linearly, there is no

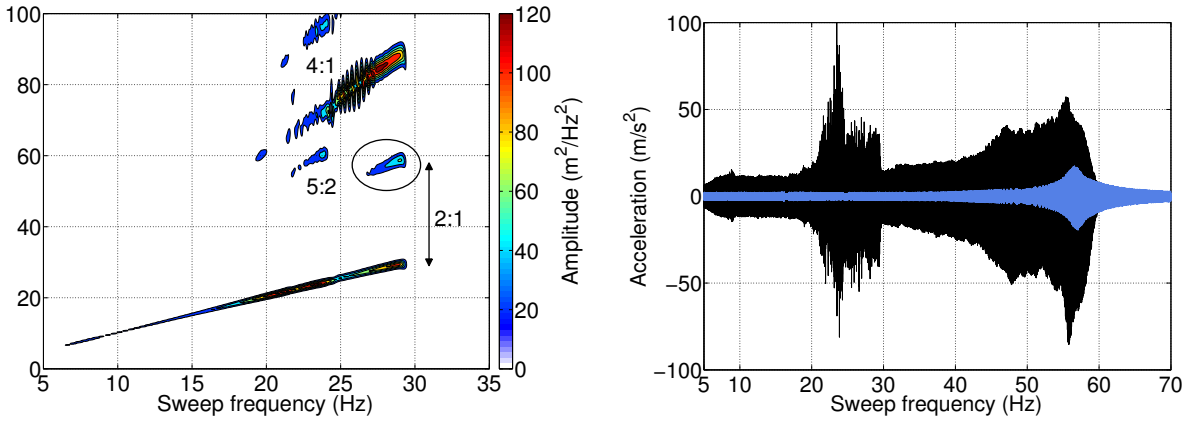

(a) (b)

Figure 6: (a) Evidence of nonlinear modal interactions using the WT calculated at NC 4 in the Z direction, and presented in 5 – 35 Hz in linear scaling. A 2:1 modal interaction between modes 3 and 7 is encircled; (b) confirmation of the existence of the 2:1 modal interaction through the raw acceleration measured at the center of the instrument panel at 0.1 g (in blue) and 1 g (in black).

sign of the 2:1 modal interaction, proving that it is an inherently nonlinear phenomenon activated for sufficiently large energies.

It should also be stressed that this 2:1 modal interaction may jeopardize the integrity of the structure as it is accompanied by an energy transfer from a local mode of the spacecraft with low effective mass, *i.e.* mode 3, to a global mode with high effective mass, *i.e.* mode 7. In addition, the time series at 1 g in Fig. 6 (b) shows that the nonlinear resonance involving the instrument panel is associated with larger accelerations (*i.e.*, 100 m/s^2) than the linear resonance of the panel (*i.e.*, 80 m/s^2). This implies that important, and potentially dangerous, dynamical phenomena can be missed when ignoring nonlinearity.

5. PARAMETER ESTIMATION IN THE PRESENCE OF NONLINEARITY

Based on the choice made in Section 4 to use trilinear functional forms to characterize the WEMS elastic behavior together with linear damping properties, the last step toward the establishment of a nonlinear model with good predictive capabilities is the estimation of the associated parameters, *i.e.* the clearances, stiffness and damping coefficients. It turns out from a survey of the technical literature [KWVG06] that the RFS method is one of the only approaches compatible with unmeasured base-sine excitations.

Though it was shown to extend to multi-DOF systems, the utilization of the RFS method is in general limited to small-scale structures, since the starting point of the approach is a rigorous writing of Newton's second law of dynamics. In Ref. [NRK14], it is however demonstrated that the equations of motion of the WEMS mobile part can be formulated explicitly by asserting that it behaves as a rigid body. The dynamics of a rigid body is known to obey 6 scalar equations, namely 3 equations describing the translation of its center of gravity, and 3 equations governing the rotation of the body around the center of gravity. One herein concentrates on the translation along Z-axis of the center of gravity of WEMS mobile part. Under the rigidity assumption, the corresponding equation of motion writes

$$m\,\frac{\ddot{z}_1+\ddot{z}_2}{2}+f_{NC\,1}(z_1)+c_1\,\dot{z}_1+f_{NC\,2}(z_2)+c_2\,\dot{z}_2=0 \tag{4}$$

where m is the mass of the WEMS mobile part estimated at 8.75 kg, $f_{NC\,1}$ and $f_{NC\,2}$ the trilinear stiffness forces, c_1 and c_2 the linear damping coefficients of the NC 1 and NC 2 elastomer plots, respectively, and where the contributions related to NC 3 and NC 4 are neglected as they involve considerably lower displacements and velocities. This results from the swing motion of the WEMS around Y-axis observed in the frequency band of interest (see Fig. 3 in Section 2).

The restoring force surfaces constructed via Eq. (4) at NC 1 and NC 2 given the triplets (z_1, $\dot{z}_1$, $f_{NC\,1}+c_1\,\dot{z}_1$) and (z_2, $\dot{z}_2$, $f_{NC\,2}+c_2\,\dot{z}_2$), respectively, can be fitted using a trilinear model in stiffness and a linear model in damping. Curve-fitting results are given in Table 3, and were computed in the 8.5 – 9 Hz interval in which the first resonance of the system is located. The damping coefficients of the elastomer plots are found to be much larger than their reference value of 63 Ns/m (see Table 1), but are prone to significant uncertainty as they were computed from a limited number of low-displacement samples. As an illustration, the stiffness curve extracted as a cross section of the corresponding restoring force surface at NC 1

	Reference value	NC 1	NC 2
Linear damping coefficient c (Ns/m)	63	218.29	147.75
Linear stiffness coefficient k	8	8.30	9.21
Neg. clearance	1.5	1.01	0.84
Pos. clearance	1.5	1.55	1.62
Neg. nonlinear stiffness coefficient	100	118.07	116.73
Pos. nonlinear stiffness coefficient	100	79.40	88.41

Table 3: Damping coefficients, stiffness coefficients and clearances of NC 1 and NC 2 estimated using the RFS method and compared with their reference values.

is plotted in Fig. 7, together with the fitted trilinear model. The calculated coefficients show that the stiffnesses of the elastomer plots and mechanical stops match well their reference values of 8 and 100 (see Table 1), respectively, considering that no asymmetry was introduced in the reference model. Impacts are also found to be comparatively softer for positive displacements.

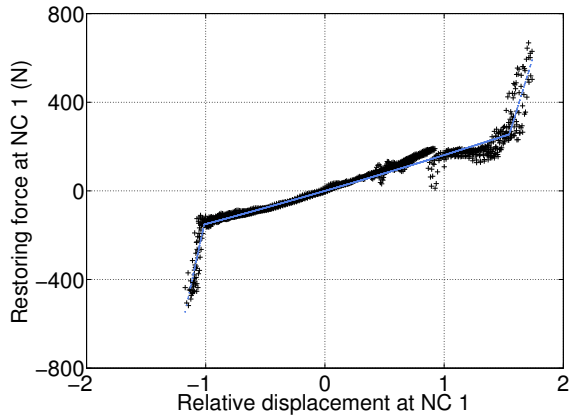

Figure 7: WEMS nonlinear stiffness curve constructed based upon Eq. (4) (in black) and compared with the fitted trilinear model (in blue) at NC 1.

6. CONCLUSION

In this paper, the experimental identification of a real-life spacecraft structure exhibiting strongly nonlinear dynamics due to multiple mechanical stops was achieved based on sine-sweep data. The complete progression through nonlinearity detection, characterization and parameter estimation was carried out by means of several existing analysis techniques, yielding an accurate estimation of the clearances and nonlinear stiffness properties of the nonlinear components. Moreover, this paper demonstrated that the complex dynamics that can be obtained during numerical simulations of nonlinear systems with low dimensionality can also be observed in experimental conditions commonly endured by engineering structures in industry. This includes intrinsically nonlinear, and potentially dangerous, phenomena such as jumps and modal interactions.

ACKNOWLEDGMENTS

This paper was prepared in the framework of the European Space Agency (ESA) Technology Research Programme study “Advancement of Mechanical Verification Methods for Non-linear Spacecraft Structures (NOLISS)” (ESA contract No.21359/08/NL/SFe). Experimental data were measured by EADS-Astrium and LMS International. The authors also thank Astrium SAS for sharing information about the SmallSat spacecraft. The authors J.P. Noël and L. Renson are Research Fellows (FRIA fellowship) of the *Fonds de la Recherche Scientifique – FNRS* which is finally gratefully acknowledged.

REFERENCES

[KPGV09] G. Kerschen, M. Peeters, J.C. Golinval, and A.F. Vakakis. Nonlinear normal modes. Part I: A useful framework for the structural dynamicist. *Mech. Syst. Signal Pr.*, 23(1):170–194, 2009.

[KWVG06] G. Kerschen, K. Worden, A.F. Vakakis, and J.C. Golinval. Past, present and future of nonlinear system identification in structural dynamics. *Mech. Syst. Signal Pr.*, 20:505–592, 2006.

[NRK14] J.P. Noël, L. Renson, and G. Kerschen. Complex dynamics of a nonlinear aerospace structure: Experimental identification and modal interactions. *J. Sound Vib.*, 333:2588–2607, 2014.

[RNK14] L. Renson, J.P. Noël, and G. Kerschen. Dynamics of a strongly nonlinear spacecraft structure. Part II: Modal analysis. In *Proc. of the Eur. Conf. on Spacecraft Structures, Materials and Environmental Testing*, Braunschweig, Germany, 2014.

[Sta00] W. J. Staszewski. Analysis of non-linear systems using wavelets. *P. I. Mech. Eng. B-J. Eng.*, 214(11):1339–1353, 2000.